

# Rethinking Diffusion for Text-Driven Human Motion Generation

Zichong Meng

Yiming Xie

Xiaogang Peng

Zeyu Han

Huaizu Jiang

Northeastern University

<https://neu-vi.github.io/MARDM/>

## Abstract

Since 2023, Vector Quantization (VQ)-based discrete generation methods have rapidly dominated human motion generation, primarily surpassing diffusion-based continuous generation methods in standard performance metrics. However, VQ-based methods have inherent limitations. Representing continuous motion data as limited discrete tokens leads to inevitable information loss, reduces the diversity of generated motions, and restricts their ability to function effectively as motion priors or generation guidance. In contrast, the continuous space generation nature of diffusion-based methods makes them well-suited to address these limitations and with even potential for model scalability. In this work, we systematically investigate why current VQ-based methods perform well and explore the limitations of existing diffusion-based methods from the perspective of motion data representation and distribution. Drawing on these insights, we preserve the inherent strengths of a diffusion-based human motion generation model and gradually optimize it with inspiration from VQ-based approaches. Our approach introduces a human motion diffusion model enabled to perform bidirectional masked autoregression, optimized with a reformed data representation and distribution. Additionally, we also propose more robust evaluation methods to fairly assess different-based methods. Extensive experiments on benchmark human motion generation datasets demonstrate that our method excels previous methods and achieves state-of-the-art performances.

## 1. Introduction

In this paper, we study the problem of human motion generation from the textual prompt (e.g., a person walks). Due to the remarkable performance in the image generation domain [18, 34, 36], diffusion models are largely adopted for human motion generation starting with the pioneer methods [20, 39, 44]. Compared with RNN [35]-based generation methods [1, 2, 11, 24], diffusion-based models offer a simpler training objective and improved stability.

In 2023, the exploration of Vector Quantization (VQ)

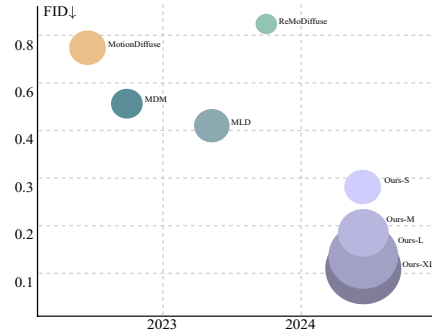


Figure 1. **HumanML3D FID results.** Each bubble’s area is proportional to the model size. We achieve superior performance and demonstrate model scalability with a diffusion-based approach.

techniques for human motion representation becomes increasingly dominant, marked a noticeable shift in attention away from diffusion models for the human motion generation task [12, 13, 43]. These methods transform continuous motion representations (e.g. processed joint positions) into discrete tokens, which enables the use of already proven generative architectures [3, 8, 42] and their training and sampling techniques from the field of natural language processing with minimal modifications.

Despite the improvement in performance, VQ-based methods still exhibit notable limitations. Representing continuous motion data as limited groups of discrete tokens inherently causes a loss of motion information, reduces generation diversity, and limits their ability to serve as motion priors or generation guidance (e.g., in the generation of dual-human motion and human-object interactions). Moreover, unlike language models, these discrete tokens often lack sufficient contextual richness affecting model scalability.

In contrast, the continuous space nature of diffusion-based generation methods can effectively address these limitations and offers potential for model scalability demonstrated by many image diffusion models [22, 28], making it an appealing alternative. In light of these, researchers have started to revisit diffusion-based approaches [45, 47]. However, these attempts struggle to achieve comparable performance to VQ-based methods. More importantly, the reasons for the performance gap between VQ and diffusion-

based human motion generation methods remain unclear.

In this work, we first systematically investigate why VQ-based motion generation approaches perform well and explore the limitations of diffusion-based methods from the perspective of motion data representation and distribution. Specifically, we: (1) Examine how VQ-based discrete formulations benefit from training with current motion data representations consisting of redundant dimensions while existing diffusion models are hindered by this data composition and its distribution. (2) Explore how VQ-based methods inherently align with current evaluation metrics, which incorporate the entire data representation including redundant dimensions, whereas diffusion-based methods are often penalized under these evaluation criteria.

Based on our diagnostic findings and inspirations from current VQ-based approaches, we aim to close the performance gap by gradually enhancing a diffusion-based model tailored for human motion generation. We first restructure the motion data representation by excluding redundant information and processing it through a 1D ResNet [15]-based AutoEncoder to achieve a distribution more compatible with diffusion models. This restructuring also improves per-frame smoothness and opens possibilities for diffusion genres beyond DDPM [18]. Additionally, we build a diffusion-based motion generation model with bidirectional masked autoregressive strategies. Finally, we propose more robust evaluators that provide unbiased assessments of the different approaches.

We summarize our contributions as follows:

- We systematically compare and investigate the reasons why VQ-based methods outperform diffusion-based methods from motion data representation and distribution perspective, providing analysis with theoretical and experimental support.
- Based on our findings and VQ-based model inspirations, we propose a scalable bidirectional masked autoregressive diffusion-based generation framework that leverages reformed data representation and distribution, evaluated with more robust evaluation methods.
- Our method achieves new state-of-the-art performance on text-to-motion generation task, with significant improvements on both KIT-ML [32] and HumanML3D [11] datasets.

## 2. Diagnosis: Motion Data Representation and Distribution

In this section, we systematically analyze how motion representation and distribution impact training, sampling (Sec. 2.2), and evaluation robustness (Sec. 2.3), revealing why these factors favor VQ-based methods while limiting diffusion-based approaches.

### 2.1. Preliminary

**VQ-based Human Motion Generation Methods.** The VQ-based methods primarily adopt two types of Vector Quantized-Variational AutoEncoders (VQ-VAEs)[41]: a standard VQ-VAE[43] or residual (R) VQ-VAE [13], to transform motion data into discrete tokens.

Given a motion sequence  $\mathbf{x}^{1:N} \in \mathbb{R}^{N \times D}$  of length  $N$ , the transformation begins by encoding  $\mathbf{x}^{1:N}$  into a latent sequence  $\mathbf{h}^{1:n} \in \mathbb{R}^{n \times d}$  with a 1D convolutional encoder  $E$ . For vanilla VQ-VAE, each vector is quantized via a base layer VQ codebook to the nearest token. In RVQ-VAE,  $V$  additional residual quantization layers are used with each residual layer quantifying the difference between the original latent vector and the quantized representation from the preceding layers. The indices  $k$  from the base layer (VQ-VAE) or all layers (RVQ-VAE) form discrete inputs for training generative models with sequence generation.

The generated discrete sequence  $\mathbf{g} = \mathbf{g}_{0:n}$  (or  $\mathbf{g}_{0:n}^{0:V+1}$  in residual case) is embedded via the codebook, then projected back (or summed then project in residual case) with an up-sample convolutional decoder  $D$  to obtain the final motion.

**Diffusion-based Human Motion Generation Methods.** The diffusion-based methods use an interpolation function,  $\mathbf{x}_t = \alpha \mathbf{x}_0 + \sigma \epsilon$ , to combine ground truth (GT) motion data with Gaussian noise  $\epsilon$  for a noisy motion  $\mathbf{x}_t$ . In motion generation, typically following DDPM [18], this function is defined as:

$$\mathbf{x}_t = \sqrt{\bar{\alpha}_t} \mathbf{x}_0 + \sqrt{1 - \bar{\alpha}_t} \epsilon \quad (1)$$

$\bar{\alpha}_t$  controls the pace of the diffusion process where  $0 = \bar{\alpha}_T < \dots < \bar{\alpha}_0 = 1$  with assumption that  $\mathbf{x}_T \sim \mathcal{N}(\mathbf{0}, \mathbf{I})$ .

During training, the model learns to predict a continuous vector from  $\mathbf{x}_t$  given  $t$ , usually the noise  $\epsilon$  or original motion  $\mathbf{x}_0$ , and is optimized with a mean squared error(MSE) loss between the predicted value and its ground truth.

During sampling, starting from random noise  $\mathbf{x}_T \sim \mathcal{N}(0, \mathbf{I})$ , for each  $t$ , the model with  $\mathbf{x}_t$  as input, predicts the original motion  $\mathbf{x}_0$  or the noise  $\epsilon$  (then to  $\mathbf{x}_0$  with Eq. (1)), and deduces intermediate samples  $\mathbf{x}_{t-1}$  (for  $t \in 1$  to  $T$ ) as:

$$\frac{\sqrt{\bar{\alpha}_t}(1 - \bar{\alpha}_{t-1})}{1 - \bar{\alpha}_t} \mathbf{x}_t + \frac{\sqrt{\bar{\alpha}_{t-1}}(1 - \alpha_t)}{1 - \bar{\alpha}_t} \mathbf{x}_0 + \sqrt{1 - \bar{\alpha}_t} \epsilon_t \quad (2)$$

where  $\epsilon_t \sim \mathcal{N}(0, \mathbf{I})$ , until it reaches the clean motion  $\mathbf{x}_0$ .

**Motion Data Representation.** The majority of recent methods utilize the canonical pose representation introduced by [11] on widely-used datasets, including KIT-ML [32] and HumanML3D [11]. This representation at a given time position  $i$  is defined as  $\mathbf{x}^i = [\dot{r}^a, \dot{r}^{xz}, \dot{r}^h, j^p, j^v, j^r, c^f]$ , comprising seven feature components: root angular velocity  $\dot{r}^a$ , root linear velocities  $\dot{r}^{xz}$  in the XZ-plane, root height  $\dot{r}^h$ , local joint positions  $j^p \in \mathbb{R}^{3(N_j-1)}$ , local velocities  $j^v \in \mathbb{R}^{3(N_j-1)}$ , joint rotations  $j^r \in \mathbb{R}^{6(N_j-1)}$  in local space, and binary foot-ground

Table 1. **Impact of Redundant Features on VQ-based Models.** VQ-based methods, T2M-GPT and Momask, trained with redundant features exhibit better reconstruction performance and lead to better generation quality on HumanML3D dataset.

Method	Trained With Redundancy	FID ↓		R-Precision ↑		
		Recon	Gen	Top 1	Top 2	Top 3
T2M-GPT [43]	✓	0.081	0.335	0.470	0.659	0.758
T2M-GPT [43]	✗	0.095	0.418	0.466	0.653	0.753
Momask [13]	✓	0.029	0.116	0.490	0.687	0.786
Momask [13]	✗	0.030	0.200	0.485	0.681	0.782

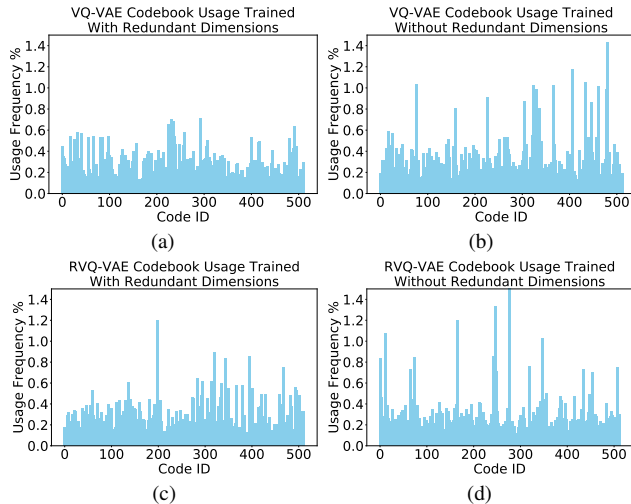


Figure 2. **Code Usage of VQ-VAEs** trained with redundancy are more balanced than VQ-VAEs trained with only essential features.

contact features  $c^f \in \mathbb{R}^4$ , where  $N_j$  denotes the joint number. However, only the first 4 feature groups from this over-parameterized representation are used to produce final human motion, making the remaining 3 components redundant.

## 2.2. Impacts on Training and Sampling

In this section, we present how this motion representation and distribution impact VQ and diffusion-based methods.

**Benefiting VQ-Based Methods.** The redundancy in data representation benefits VQ-VAE training which then enhances discrete generation modeling. To validate this viewpoint, we conduct controlled experiments by training VQ-VAE from T2M-GPT [43] and RVQ-VAE from MoMask [13] on HumanML3D with and without redundancy, and then train each generative models following original methods. As shown in Tab. 1, training with redundant dimensions results in significantly better VQ-VAEs which subsequently enhance the performance of discrete generative models. To understand the reason, we further analyze their role in VQ-VAE training.

Let  $\mathbf{x}_r^{\text{GT}}$  and  $\mathbf{x}_e^{\text{GT}}$  denote the ground truth data with and without redundancy and  $\mathbf{x}_r^{\text{pred}}$  and  $\mathbf{x}_e^{\text{pred}}$  represent the prediction. The reconstruction loss  $\mathcal{L}_r^{\text{rec}}$  and  $\mathcal{L}_e^{\text{rec}}$  with and without

Table 2. **The results of MDM on humanML3D dataset.** We report the results of MDM with original  $\mathbf{x}_0$  prediction vs. with  $\epsilon$  prediction. Training to predict  $\mathbf{x}_0$  leads to significant better results

Method	Prediction	FID ↓		R-Precision ↑		
		Gen	Top 1	Top 2	Top 3	
MDM-50Step [39]	$\mathbf{x}_0$	0.518	0.440	0.636	0.742	
MDM-50Step [39]	$\epsilon$	31.265	0.054	0.103	0.147	

redundancy, typically measured with variation of  $L_1$  or  $L_2$  loss can be decomposed as:

$$\begin{aligned} L_r^{\text{rec}} &= \mathcal{L}(\mathbf{x}_e^{\text{GT}} - \mathbf{x}_e^{\text{pred}} + \mathbf{x}_{r-e}^{\text{GT}} - \mathbf{x}_{r-e}^{\text{pred}}) \\ &= L_e^{\text{rec}} + \mathcal{L}(\mathbf{x}_{r-e}^{\text{GT}} - \mathbf{x}_{r-e}^{\text{pred}}). \end{aligned} \quad (3)$$

showing the redundancy acts as a data-level regularization

This built-in regularization helps reduce model variance, producing representations less sensitive to fluctuations in training data, leading to better generalization which ultimately enhances codebook usage and consistency. As shown in Fig. 2 on the HumanML3D test set, both VQ-VAE and RVQ-VAE and models trained with redundant dimensions exhibit more uniform code utilization while models trained without redundancy show distinct spikes in certain codes meaning overfitting, demonstrating the benefit of incorporating redundant dimensions for VQ-based methods.

**Limiting Diffusion-Based Methods.** The current data representation and distribution impose constraints on the modeling approaches for diffusion-based methods.

Most diffusion-based methods follow the DDPM [18] but predict original motion  $\mathbf{x}_0$ . Attempts to train these methods to predict noise often fail, e.g. MDM [39] in Tab. 2. This deterministic  $\mathbf{x}_0$ -only prediction in each timestep also limits training simplicity and sampling diversity.

Below, we outline how current motion data constrains diffusions to learn and sample only  $\mathbf{x}_0$ : dimensional distribution mismatch and error amplification with  $\epsilon$  prediction.

First, the current motion data may not follow a standard normal distribution with standard z-normalization due to its mixed structure consisting of features from 3D continuous, 6D rotatory (e.g. joint rotation), and categorical (e.g. foot contacts) distribution. This leads to a dimensional distribution mismatch and challenges the interpolation function (Eq. (1) for DDPM). In the forward diffusion process, due to the differing initial distributions of  $\mathbf{x}_0$ 's different feature groups, feature groups of  $\mathbf{x}_T$  may converge to their own distinct distribution by time step  $T$ , rather than all converging to a standard normal distribution. Consequently, in the reverse diffusion process, starting from a standard normal distribution, which the model is not trained to predict from, leads to errors in motion generation.

Second, consider two main data processing methods: (1) standard z-normalization, followed by averaging the standard deviation (SD)  $\sigma^x$  for each 7 feature groups, (2) additionally, scaling the SD by a feature bias term. In the first method, the averaged SD  $\sigma^x$  for a group with  $D$  di-

Table 3. **Existing Evaluator performance** results with altering HumanML3D data by adding noise or replacing with noise in essential and redundant dimensions. The evaluator heavily emphasizes redundant dimensions during evaluation process.

Dimension	Method	FID ↓		R-Precision ↑	
		Gen	Top 1	Top 2	Top 3
Essential	Add Noise	2.021	0.442	0.634	0.740
Redundant	Add Noise	21.032	0.310	0.471	0.575
Essential	Replace W/ Noise	15.164	0.264	0.425	0.538
Redundant	Replace W/ Noise	38.167	0.154	0.257	0.336

mensions is:  $\sigma'^{\mathbf{x}} = \frac{\sum_{i=0}^{D-1} \sigma_i^{\mathbf{x}}}{D}$  with the ratio  $\phi'^{\mathbf{x}}$  of original (which is also  $\epsilon$ 's SD =  $\mathbf{I}$ ) to adjusted SD as  $\phi'^{\mathbf{x}} = \frac{\sigma'^{\mathbf{x}}}{\sigma^{\mathbf{x}}}$ . In the second method, this ratio is further adjusted by a feature bias term  $\gamma$ :  $\phi'^{\mathbf{x}} = \gamma \times \frac{\sigma'^{\mathbf{x}}}{\sigma^{\mathbf{x}}}$ .

Unlike predicting  $\mathbf{x}_0$ , where the error is standardized to predicted  $\mathbf{x}_0$  and its ground truth in each timestep, this SD ratio will cause error amplification when predicting noise.

Suppose  $\epsilon_\theta(\mathbf{x}_t, t)$  denote the predicted noise  $\epsilon$  at time  $t$  and define  $\delta_{\mathbf{x}_0}$  as the squared error between ground truth and predicted  $\mathbf{x}_0$ , and  $\delta_\epsilon$  as the error for noise prediction. Then we have  $\delta_\epsilon = \|\epsilon_\theta(\mathbf{x}_t, t) - \epsilon\|_2^2$  and  $\delta_{\mathbf{x}_0} = \left\| \frac{1}{\sqrt{\bar{\alpha}_t}} (\mathbf{x}_t - \sqrt{1 - \bar{\alpha}_t} \epsilon_\theta(\mathbf{x}_t, t)) - \mathbf{x}_0 \right\|_2^2$ . Substitute  $\mathbf{x}_0$  from Eq. (1) (detailed deduction in App. A.1), we get:

$$\delta_{\mathbf{x}_0} = \left\| \frac{1 - \bar{\alpha}_t}{\bar{\alpha}_t} \right\|_2^2 \delta_\epsilon, \quad (4)$$

an standard error relation  $\delta_\epsilon \rightarrow \delta_{\mathbf{x}_0}$  if  $\mathbf{x}_0$  is processed correctly which only responds to time coefficient  $\bar{\alpha}$ . Since the SD ratio  $\phi'^{\mathbf{x}}$  applies to both deduced and ground truth  $\mathbf{x}_0$ , then Eq. (4) updates to:

$$\delta_{\mathbf{x}_0} \times \phi'_i = \left\| \frac{\sqrt{1 - \bar{\alpha}_t}}{\sqrt{\bar{\alpha}_t}} \right\|_2^2 \delta_\epsilon. \quad (5)$$

where  $\bar{\alpha}$  remains unchanged and  $\epsilon$  guaranteed from normal distribution. This means unlike direct  $\mathbf{x}_0$  prediction, errors from predicting  $\epsilon$  are actually amplified because of the modified SD and are worsened by feature bias.

Both dimensional distribution mismatch and noise prediction error amplification can seriously impact generation. Therefore, reformatting motion representation and distribution is crucial to improve motion diffusion modeling.

### 2.3. Impact on Method Evaluation Robustness

The widely adopted evaluators [11] utilize all features including redundant 3 components which can be imprecise and unfair.

To assess this, we conducted an experiment by selectively altering redundant and non-redundant dimensions of ground truth HumanML3D data to examine their impact on the evaluator. As shown in Tab. 3, the evaluator disproportionately emphasizes redundant dimensions, potentially misclassifying accurate human motion as poor if minor imperfections exist in redundancy.

Table 4. **The evaluation results using evaluators trained on all vs. essential dimensions on HumanML3D data.** VQ-based models perform similarly with both evaluators, while diffusion-based models are disadvantaged when evaluated with redundancy.

Method	Evaluator With Redundancy	FID ↓		R-Precision ↑		
		Gen	Top 1	Top 2	Top 3	
T2M-GPT [43]	✓	0.115	0.497	0.685	0.779	
Momask [13]	✓	0.093	0.508	0.701	0.796	
MDM-50Step [39]	✓	0.481	0.459	0.651	0.753	
T2M-GPT [43]	✗	0.335	0.470	0.659	0.758	
Momask [13]	✗	0.116	0.490	0.687	0.786	
MDM-50Step [39]	✗	0.518	0.440	0.636	0.741	

**Benefiting VQ-Based Methods.** The VQ codebooks enforce a discrete one-to-one token-to-embedding mapping, ensuring error consistency across both essential and redundant dimensions, ultimately advantage VQ-based methods under evaluators that account for all dimensions.

Unlike traditional VAEs [21], where the continuous latent space can lead to projected output dimensional inconsistencies, VQ-VAEs establish a one-to-one correspondence between each code and its embedding. While this approach may limit data diversity, the deterministic mapping constrains outputs to a defined set of embeddings, producing stable features across all dimensions. Mathematically, each VQ codebook embedding  $e_k$  represents a Voronoi cell:

$$V_k = \{z \in \mathbb{R}^d \mid \|z - e_k\|_2 \leq \|z - e_j\|_2, \forall j \neq k\}. \quad (6)$$

Generation error then corresponds to errors of cell centroids, yielding a more uniform error rate across dimensions and aligning well with evaluators that assess all dimensions.

**Limiting Diffusion-Based Methods.** The continuous predictions nature of diffusion-based methods causes error inconsistency in each dimension, hindered in evaluation.

In each timestep, diffusion-based models predict a continuous vector to recover  $\mathbf{x}_0$  without dimension alignment, introducing variability across individual dimensions. As iteration continues, these dimensional fluctuations accumulate. We can express the total error with diffusion model  $f$ :

$$\text{Total Error} = \sum_{t=0}^T \sum_{d=1}^D \left\| f(\mathbf{x}_t^{(d)}, \epsilon_t^{(d)}) - \mathbf{x}_{\text{true}}^{(d)} \right\|_2^2 \quad (7)$$

we see each dimension contributes differently to the overall error depending on its error rate and variability across dimensions results in inconsistent error rates. Since the evaluator considers all dimensions, diffusion-based models are penalized because of error rate inconsistency, especially in the redundant dimensions, leading to unfair evaluations.

In Tab. 4, we compare model performance when evaluated on all versus essential dimensions. Results indicate that VQ-based methods exhibit more consistent error across dimensions, benefit from all-dimension evaluation. Diffusion-based methods, despite excelling in essential dimensions, are penalized for fluctuation in redundant dimensions. This underscores a more robust evaluator is crucial.

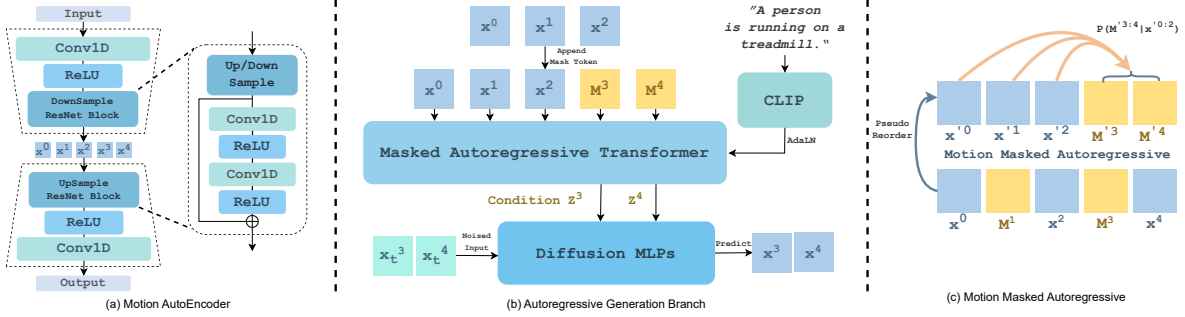


Figure 3. **Method Overview.** (a) The reformed motion sequence is projected into a compact fine-grained latent space through a Motion AutoEncoder. (b) The motion latents  $\mathbf{x}^{0:3}$  are processed through a Masked Autoregressive Transformer, where they are either randomly masked (in training) or appended (in inference) with a learnable mask vector (yellow-colored latents). The transformer provides a condition  $z$  for the masked positions to the Diffusion MLPs to produce clean latent  $\mathbf{x}^{3:4}$  from the noised input. (c) A visual illustration of motion masked autoregressive where masked latents (yellow-colored) can be reordered into a pseudo-position allowing  $p(m^{3:4} | \mathbf{x}^{0:2})$  prediction.

### 3. Revisiting Motion Diffusion

Guided by the insights from Sec. 2 and inspirations from VQ-based methods, we revisit diffusion-based human motion generation in this section and present a new method. It does not only overcome the limitations we found in Sec. 2 but also leverages the strengths of autoregressive generation, leading to a new state-of-the-art model.

#### 3.1. Reforming Motion Representations

To systematically address the limitations of motion representations in Sec. 2.2, we use only the essential feature groups (*i.e.*, the first  $\#\text{joints} \times 3 + 1$  dimensions). After excluding the redundant dimensions, we avoid mixing representations from various distributions, such as 6D rotational and categorical. The retained features are all 3D continuous representations, ensuring a uniform distribution that aligns better with diffusion-based generation framework.

To further optimize the motion representations, we then project those essential features into a compact and fine-grained latent space using a motion AutoEncoder (AE). Compared with the motion Variational AutoEncoder (VAE) [5], the deterministic AE projection avoids the variation in the motion latents (*i.e.*  $\epsilon$  incorporation), providing more stable representations that are better suited for diffusion modeling and motion reconstruction.

The AE architecture is shown in the left-most part of Fig. 3, where the motion sequence with essential representations  $\mathbf{X}^{0:N}$  is projected into a latent space using a 1D ResNet [15]-based encoder  $E$ . This latent embedding  $\mathbf{x}^{0:n}$  then passes through a 1D ResNet decoder  $D$ , which uses nearest-neighbor upsampling to reconstruct the motion feature  $\mathbf{X}^{0:N}$ . Formally, the training loss of AE is defined as:

$$\mathcal{L}_{\text{ae}} = \|\mathbf{X}^{0:N} - \mathbf{X}'^{0:N}\|_1. \quad (8)$$

Following previous works using latent space [5, 13, 43], the encoder  $E$  downsamples  $\mathbf{X}$  from  $N$  length to  $\mathbf{x}$  of  $n$  length. The decoder  $D$  upsamples it back to  $N$  length. With this

integration, our method can also use motion latent  $\mathbf{x}$  in the diffusion process, which offers acceleration for both training and sampling. In addition, since the downsampling introduces temporal awareness [11], it can improve the temporal coherence of autoregressive diffusion in Sec. 3.2.

More importantly, since our reformed motion representations can effectively address the issues highlighted in Sec. 2.2, it free diffusion models from the constraint of predicting only  $\mathbf{x}_0$  to  $\epsilon$  and more advanced diffusion predictions are now feasible, *e.g.* score and velocity. Following SiT [25], we define a linear interpolation function as:

$$\mathbf{x}_t = \alpha_t \mathbf{x}_0 + \sigma_t \epsilon = (1 - t)\mathbf{x}_0 + t\epsilon, \quad (9)$$

where  $t$  is the continuous timestep. Then the velocity for diffusion to predict is defined as:

$$\mathbf{v}(\mathbf{x}, t) = \dot{\alpha}_t \mathbb{E}[\mathbf{x}_0 | \mathbf{x}_t = \mathbf{x}] + \dot{\sigma}_t \mathbb{E}[\epsilon | \mathbf{x}_t = \mathbf{x}]. \quad (10)$$

The score is another form of velocity:

$$\mathbf{s}(\mathbf{x}, t) = \sigma_t^{-1} \frac{\alpha_t \mathbf{v}(\mathbf{x}, t) - \dot{\alpha}_t \mathbf{x}}{\dot{\alpha}_t \sigma_t - \alpha_t \dot{\sigma}_t}, \quad (11)$$

where  $\alpha_t, \sigma_t$  are continuous time coefficients,  $\dot{\alpha}_t = \frac{d\alpha_t}{dt}$ ,  $\dot{\sigma}_t = \frac{d\sigma_t}{dt}$ . We can also deduce the score  $\mathbf{s}(\mathbf{x}, t)$  from  $\mathbf{v}(\mathbf{x}, t)$  if needed.

#### 3.2. Diffusion: An Autoregressive Approach

Autoregressive methods [13, 30, 31, 43] demonstrate significant advantages in motion generation. Instead of generating the entire sequence  $\mathbf{x}^{1:n}$  with a condition  $c$  by modeling  $p(\mathbf{x}^{1:n} | c)$ , autoregressive generation defined as ‘‘predicting next token/tokens with previous token/tokens’’, simplify the generation process as sequentially generating continuations through chains:

$$p(\mathbf{x}^{1:n} | c) = p(\mathbf{x}^1 | c) \prod_{i=1}^n p(\mathbf{x}^i | \mathbf{x}^{<i}), \quad (12)$$

where each conditional probability  $p(\mathbf{x}^i | \mathbf{x}^{<i})$  represents the likelihood of generating motion  $\mathbf{x}_i$  given previous ones  $\mathbf{x}^{<i}$ .

Naively training diffusion models to perform autoregressive generation using MSE loss between the model output and ground truth fails as it simplifies to a regression problem rather than explicitly capturing the chained probabilistic distributions of  $p(\mathbf{x}^{1:n}|c)$  in autoregressive generation.

Inspired by recent image generation advances [22, 40], which demonstrate the potential of autoregressive continuous image modeling by leveraging logits from an autoregressive model as conditioning parameters into a continuous sampling network to better model underlying probability, we revisit human motion diffusion models from an autoregressive perspective, leveraging its advantages of simplified generation process as chained continuations.

### 3.2.1 Masked Autoregressive Motion Generation

We follow the masked autoregressive approach proposed by MAR [22]. For human motion generation, in each autoregressive iteration, we define unmasked motion latents as  $\text{um} = \mathbf{x}^{i_1:i_k}$  and masked motion latents as  $\text{m} = \mathbf{x}^{j_1:j_{n-k}}$ . The unmasked latents can be refined in a new pseudo-order  $\text{um} = \mathbf{x}^{1:k}$  to serve as previously generated blocks, and the masked motion latents  $\text{m} = \mathbf{x}^{k+1:n}$  represent the motion latents that need to be generated based on  $\text{um}$  with condition  $c$ . Formally, this process is  $p(\mathbf{x}^{1:n}|c) =$

$$p(\text{m}|c) \prod_{j=1}^k p(\text{m}|\text{um}) \quad (13)$$

where  $k$  is number of autoregressive steps needed to produce the entire sequence. we also visually illustrate motion masked autoregressive in the right-most part of Fig. 3.

### 3.2.2 Autoregressive Generation Branch

Our proposed autoregressive diffusion generation architecture is shown in the middle of Fig. 3. It consists of two major parts: a Masked Autoregressive Transformer and per-latent Diffusion Multi-Layer Perceptions (MLPs).

**Masked Autoregressive Transformer** is designed to process time-variant motion data and provide rich contextual condition  $z$  for the diffusion branch. Given unmasked motion latent sequence  $\text{um}$  as previous generated motion latents, the masked autoregressive transformer  $g$  will produce conditions  $z$  to the diffusion branch to generate latents at position of masked motion latents  $\text{m}$  by:

$$z = g(\text{um}). \quad (14)$$

Given the relative simplicity of motion data compared to image data, we choose to incorporate a single AdaLN [14] transformer [42] layer and leverage the generation performance and speed benefits from bidirectional attention shown in many previous methods [13, 30, 31].

**Diffusion MLPs** adopts MLPs as its primary structure because with autoregressive modeling, the motion data input into the diffusion branch is independent single  $D$ -dimensional motion latents. The single  $D$ -dimensional structure input data aligns well with the MLP’s simplicity and strength in channel-wise manipulation. Unlike MAR [22], where scaling focuses on understanding models, in motions, we scale diffusion MLPs to various model sizes. Using the condition  $z$  from Masked Autoregressive Transformer, diffusion branch produce each motion latents  $\mathbf{x}^i$  in masked token  $\text{m}$ ’s position at each timestep  $t$  by:

$$\mathbf{x}_{t-1}^i \sim p(\mathbf{x}_{t-1}^i | \mathbf{x}_t^i, t, z^i) \quad (15)$$

During training, we randomly mask a subset of  $k$  motion latents with a learnable continuous mask vector following the cosine masking schedule from MoMask [13]. The autoregressive model learns to provide accurate signals on the unmasked latents given time step and text condition, with the diffusion MLPs learn to utilize this signal to predict  $\epsilon$  or  $\mathbf{v}(\mathbf{x}, t)$ . Training objectives for entire generation branch denote as:

$$\mathcal{L}_{GB} = \mathbb{E}_{\epsilon, t} \left[ \left\| \epsilon - \epsilon_{\theta}(\mathbf{x}_t^i | t, g(\text{um})) \right\|^2 \right] \quad (16)$$

modeling noise prediction. For velocity prediction,  $\mathcal{L}_{GB} =$

$$\int_0^T \mathbb{E}_{\mathbf{v}, t} \left[ \left\| \mathbf{v}_{\theta}(\mathbf{x}_t^i | t, g(\text{um})) - \dot{\alpha}_t \mathbf{x}_0^i - \dot{\sigma}_t \epsilon \right\|^2 \right] dt \quad (17)$$

During sampling, given previous latents  $\text{um}$ , we simply add mask vectors to the sequence, allowing the autoregressive model to generate appropriate signals for masked positions and feed into the diffusion MLPs to sample latents. The sampling process can be denoted as:

$$\mathbf{x}_{t-1}^i = \frac{1}{\sqrt{\alpha_t}} \left( \mathbf{x}_t^i - \frac{\sqrt{1-\alpha_t}}{\sqrt{1-\bar{\alpha}_t}} \epsilon_{\theta}(\mathbf{x}_t^i | t, z^i) \right) + \sigma_t \epsilon_t \quad (18)$$

where  $\epsilon_t \sim \mathcal{N}(\mathbf{0}, \mathbf{I})$  for noise prediction. For velocity prediction using ODE sampling with step size  $\Delta t$  then:

$$\mathbf{x}_{t-1}^i = \mathbf{x}_t^i + \Delta t \cdot \mathbf{v}_{\theta}(\mathbf{x}_t^i | t, z^i) \quad (19)$$

### 3.3. Evaluation: More Robust Evaluators.

To address biases in the current evaluation approach shown in Sec. 2.3, we propose a new evaluation framework that focuses exclusively on essential features, enabling a fairer generation evaluation across different-based methods.

We first construct an evaluator that retains the architecture of the widely used evaluator [11], consisting of a convolutional movement encoder, a GRU[6]-based motion encoder, and a GRU-based text encoder using GloVe[29] embeddings, to ensure consistency. This evaluator is trained solely on essential dimensions to prioritize features that meaningfully contribute to final motion generation.

To incorporate recent advancements, we also design a CLIP[23, 33, 38]-based evaluator trained with per-batch

	Methods	Framework	R-Precision $\uparrow$			FID $\downarrow$	Matching $\downarrow$	MModality $\uparrow$	CLIP-score $\uparrow$
			Top 1	Top 2	Top 3				
HumanML3D	T2M-GPT [43]	VQ	0.470 $\pm$ .003	0.659 $\pm$ .002	0.758 $\pm$ .002	0.335 $\pm$ .003	3.505 $\pm$ .017	2.018 $\pm$ .053	0.607 $\pm$ .005
	MMM [31]		0.487 $\pm$ .003	0.683 $\pm$ .002	0.782 $\pm$ .001	0.132 $\pm$ .004	3.359 $\pm$ .009	1.241 $\pm$ .073	0.635 $\pm$ .003
	MoMask [13]		0.490 $\pm$ .004	0.687 $\pm$ .003	0.786 $\pm$ .003	0.116 $\pm$ .006	3.353 $\pm$ .010	1.263 $\pm$ .079	<u>0.637<math>\pm</math>.003</u>
	MDM-50Step [39]	Diffusion	0.440 $\pm$ .007	0.636 $\pm$ .006	0.742 $\pm$ .004	0.518 $\pm$ .032	3.640 $\pm$ .028	<b>3.604<math>\pm</math>.031</b>	0.578 $\pm$ .003
	MotionDiffuse [44]		0.450 $\pm$ .006	0.641 $\pm$ .005	0.753 $\pm$ .005	0.778 $\pm$ .005	3.490 $\pm$ .023	3.179 $\pm$ .046	0.606 $\pm$ .004
	MLD [5]		0.461 $\pm$ .004	0.651 $\pm$ .004	0.750 $\pm$ .003	0.431 $\pm$ .014	3.445 $\pm$ .019	<u>3.506<math>\pm</math>.031</u>	0.610 $\pm$ .003
	ReMoDiffuse [45]		0.468 $\pm$ .003	0.653 $\pm$ .003	0.754 $\pm$ .005	0.883 $\pm$ .021	3.414 $\pm$ .020	2.703 $\pm$ .154	0.621 $\pm$ .003
	<b>Ours-DDPM</b>	Autoregressive	0.492 $\pm$ .006	0.690 $\pm$ .005	0.790 $\pm$ .005	0.116 $\pm$ .004	3.349 $\pm$ .010	2.470 $\pm$ .053	0.637 $\pm$ .005
<b>Ours-SiT</b>	Diffusion	<b>0.500<math>\pm</math>.004</b>	<b>0.695<math>\pm</math>.003</b>	<b>0.795<math>\pm</math>.003</b>	<b>0.114<math>\pm</math>.007</b>	<b>3.270<math>\pm</math>.009</b>	2.231 $\pm$ .071	<b>0.642<math>\pm</math>.002</b>	
KIT	T2M-GPT [43]	VQ	0.359 $\pm$ .007	0.553 $\pm$ .007	0.690 $\pm$ .013	0.593 $\pm$ .053	3.765 $\pm$ .046	1.798 $\pm$ .157	0.651 $\pm$ .005
	MMM [31]		0.363 $\pm$ .005	0.569 $\pm$ .006	0.724 $\pm$ .006	0.478 $\pm$ .034	3.629 $\pm$ .028	1.455 $\pm$ .106	0.660 $\pm$ .003
	MoMask [13]		0.369 $\pm$ .005	0.588 $\pm$ .005	0.731 $\pm$ .005	0.411 $\pm$ .026	3.577 $\pm$ .021	1.309 $\pm$ .058	0.669 $\pm$ .002
	MDM [39]	Diffusion	0.333 $\pm$ .012	0.561 $\pm$ .009	0.689 $\pm$ .009	0.585 $\pm$ .043	4.002 $\pm$ .033	1.681 $\pm$ .107	0.605 $\pm$ .007
	MotionDiffuse [44]		0.344 $\pm$ .009	0.536 $\pm$ .007	0.658 $\pm$ .007	3.845 $\pm$ .087	4.167 $\pm$ .054	1.774 $\pm$ .217	0.626 $\pm$ .006
	MLD [5]		0.351 $\pm$ .007	0.536 $\pm$ .007	0.658 $\pm$ .007	0.492 $\pm$ .047	3.746 $\pm$ .044	<u>1.803<math>\pm</math>.164</u>	0.646 $\pm$ .006
	ReMoDiffuse [45]		0.356 $\pm$ .004	0.572 $\pm$ .007	0.706 $\pm$ .009	1.725 $\pm$ .053	3.735 $\pm$ .036	<b>1.928<math>\pm</math>.127</b>	0.665 $\pm$ .005
	<b>Ours-DDPM</b>	Autoregressive	0.375 $\pm$ .006	0.597 $\pm$ .008	0.739 $\pm$ .006	0.340 $\pm$ .020	3.489 $\pm$ .018	1.479 $\pm$ .078	0.681 $\pm$ .003
<b>Ours-SiT</b>	Diffusion	<b>0.387<math>\pm</math>.006</b>	<b>0.610<math>\pm</math>.006</b>	<b>0.749<math>\pm</math>.006</b>	<b>0.242<math>\pm</math>.014</b>	<b>3.374<math>\pm</math>.019</b>	1.312 $\pm$ .053	<b>0.692<math>\pm</math>.002</b>	

Table 5. **Quantitative evaluation on HumanML3D and KIT-ML datasets.** We repeat the evaluation 20 times and report the average with 95% confidence interval. For our methods, we report both method results trained to predict noise (DDPM[18]) and velocity (SiT[25]). We use **Bold** face to indicate the best result and underscore to present the second best.

contrastive learning. Specifically, motion captions are tokenized, embedded, and processed through a transformer encoder branch, while motion data are projected and processed through another transformer encoder branch. The end-of-sentence token from the text embeddings and the CLS token from the motion embeddings are extracted to represent each modality. The model learns to align these representations by maximizing the per-batch cosine similarity between the normalized features of two modalities scaled by a learnable logit scale. This CLIP-based evaluator is also trained using only essential dimensions.

By training exclusively on essential dimensions, we ensure the evaluators capture only meaningful features from the final generated motion. The adoption of dual evaluators also provides a more robust and comprehensive framework to accurately compare different-based generation methods.

## 4. Experiment

### 4.1. Datasets and Evaluation Protocols.

**Datasets.** To accurately and fairly evaluate our method in comparison with baselines, we adopt two representative motion-language benchmarks: HumanML3D [11] and KIT-ML [32]. The KIT-ML dataset comprises 3,911 motions sourced from the KIT and CMU [27] motion data, each accompanied with one to four textual annotations (6,278 total annotations). The KIT-ML motion sequences are standardized to 12.5 FPS. The HumanML3D dataset contains 14,616 motions sourced from the AMASS [26] and HumanAct12 [10] datasets, each described by three textual scripts (44,970 total annotations). The HumanML3D motion sequences are adjusted to 20 FPS with a maximum duration of 10 seconds. We augment data by mirroring and splitting both datasets into train, test, and validation sets with a ratio

of 0.8:0.15:0.05. We follow the pose representation from T2M [10], however, we incorporate only essential dimensions for methods’ evaluation and training in our method.

**Evaluation metrics** Following Section 3.3, we employ two evaluators trained with only essential dimensions: one architecturally identical to the one proposed in T2M [11] and a CLIP-based evaluator. Using the T2M evaluator, we adopt evaluation metrics from T2M, including (1) R-Precision (Top-1, Top-2, and Top-3 accuracies) and Matching, which measures the semantic alignment between generated motion embeddings and their corresponding captions’ glove embedding; (2) Fréchet Inception Distance (FID), which assesses the statistical similarity between ground truth and generated motion distributions; and (3) Multi-Modality, which measures the diversity of generated motion embeddings per same text prompt. Using the CLIP-based evaluator, we include the CLIP-score [16], which measures the compatibility of motion-caption pairs by calculating the cosine similarity between generated motion embedding and motion caption.

### 4.2. Results and Analysis

Following previous works [11, 39], we conduct each experiment 20 times on both datasets and report the mean result along with a 95% confidence interval. To ensure a fair comparison on the new evaluators, we train all baseline models from scratch following their original methods on the same obtained dataset (full dimension). We present the quantitative results of our method alongside baseline state-of-the-art human motion generation methods in Tab. 5, and the qualitative comparison results in Fig. 4. In addition we also present model scalability results in App. C

As observed, our method achieves superior performance across multiple metrics, including FID, R-Precision,

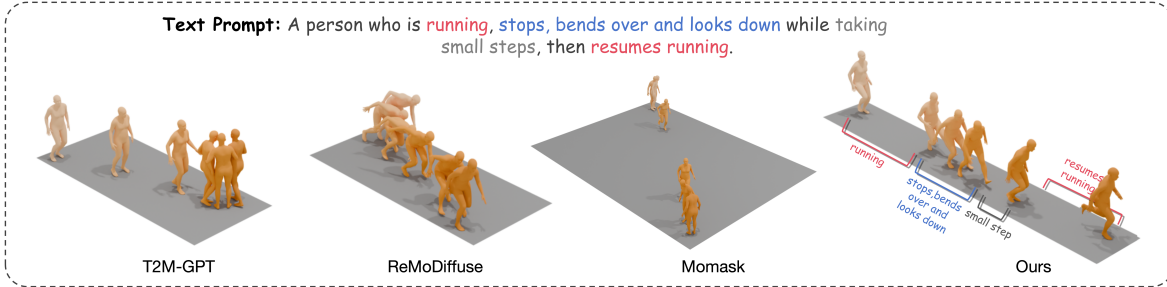


Figure 4. **Visualization Comparison** between our method and baseline state-of-the-art methods. Our method generates motion that is more realistic and more accurately follows the fine details of the textual condition.

Table 6. **Ablation study results** comparing our method to variations without reform data representation and distribution and without autoregression. The study is conducted on the HumanML3D dataset.

Method	FID ↓	R-Precision ↑		
		Top 1	Top 2	Top 3
Full Components	0.116	0.492	0.690	0.790
W/o Motion Representation Reformation	2.196	0.387	0.595	0.703
W/o Autoregression	0.551	0.435	0.621	0.732

Matching score, and CLIP-score, consistently outperforming baseline methods with non-marginal improvements on both KIT-ML and HumanML3D datasets. Compared to diffusion-based baseline methods, our approach showcases a significantly stronger ability to generate stable motion that follows closely to text instructions and aligns with ground truth. Notably, while the SOTA diffusion-based baseline method ReMoDiffuse [45] relies on additional data retrieval from a large database to achieve high-quality motion generation, our method surpasses ReMoDiffuse’s performance results without requiring auxiliary formulations. In comparison to VQ-based baseline methods, our approach maintains better motion quality and also delivers greater diversity, a quality where VQ-based methods typically underperform.

### 4.3. Ablation Study

In the ablation study, we further study the impact of reforming data representation and distribution, and autoregressive modeling in our method. We present the ablation result in Tab. 6. The results demonstrate that both these proposed components contribute greatly.

**Data Representation and Distribution** Without reform motion data representation and distribution, FID increased by 2.080, and R-precisions dropped by 8.7 percent for Top 3. Therefore, reforming data and representation is crucial.

**Autoregressive Modeling** Without autoregressive modeling, FID increased by 0.435, and R-precisions dropped by 5.8 percent for Top 3. Therefore autoregressive modeling also contributes greatly to our proposed method.

## 5. Related Work

**VQ-Based Human Motion Generation** TM2T [12] first introduces Vector Quantization (VQ) to text-to-human motion generation, enabling discrete motion token modeling. T2M-GPT [43] extended this by leveraging a GPT[3] to motion autoregressive generation. Subsequent methods have sought to integrate a larger model[19, 46] (e.g. large language models), or manipulate attention mechanisms [48]. Most recently, MMM [31] and MoMask [13] revisit generation methodology by employing bidirectional attention-based masked generation techniques inspired by MaskGIT [4]. BAMB [30] introduced a dual-iteration framework that combines unidirectional generation with bidirectional refinement to enhance the coherence of generated motions. In this paper, we examine the strengths of these approaches and improve a diffusion model inspired by these insights.

**Diffusion-Based Human Motion Generation.** Inspired by the success of denoising diffusion models in image generation domain [18, 37], several pioneering works [20, 39, 44] have adapted denoising diffusion processes to human motion generation. Building on these works, MLD [5] further optimized the denoising process in latent space to improve training and sampling efficiency. Recent methods have diversified their focus, exploring retrieval-augmentation [45], controllable generation [7], as well as investigating advanced architectures [47] such as Mamba [9]. In this paper, we thoroughly investigate the limitations of diffusion-based methods and propose a novel approach to address them.

**Autoregressive Generation with Continuous Data.** GIVT first introduced the idea of leveraging outputs from an autoregressive model as parameters for a Gaussian Mixture Model, enabling probabilistic autoregressive modeling and generation. MAR then utilized logits from a masked autoregressive model as input to a small diffusion branch, producing more fine-grained generation. Inspired by these approaches, in this paper, we propose a novel framework that integrates diffusion-based motion generation with autoregression, combining the strengths from both worlds to achieve enhanced generative performance.



## 6. Conclusion

In conclusion, we introduce a novel diffusion-based generative framework for text-driven 3D human motion generation. Our method reforms motion data representation and distribution to better fit the diffusion model, incorporated bidirectional masked autoregressive training and sampling techniques, and is evaluated by more robust evaluators. Extensive experiments demonstrate our method’s superior motion generation performance across evaluation metrics in both KIT-ML and HumanML3D datasets.

## References

- [1] Gunjan Aggarwal and Devi Parikh. Dance2music: Automatic dance-driven music generation. *arXiv preprint arXiv:2107.06252*, 2021. 1
- [2] Chaitanya Ahuja and Louis-Philippe Morency. Language2pose: Natural language grounded pose forecasting. In *2019 International Conference on 3D Vision (3DV)*, pages 719–728. IEEE, 2019. 1
- [3] Tom B Brown. Language models are few-shot learners. *arXiv preprint arXiv:2005.14165*, 2020. 1, 8
- [4] Huiwen Chang, Han Zhang, Lu Jiang, Ce Liu, and William T Freeman. Maskgit: Masked generative image transformer. In *Proceedings of the IEEE/CVF Conference on Computer Vision and Pattern Recognition*, pages 11315–11325, 2022. 8
- [5] Xin Chen, Biao Jiang, Wen Liu, Zilong Huang, Bin Fu, Tao Chen, and Gang Yu. Executing your commands via motion diffusion in latent space. In *Proceedings of the IEEE/CVF Conference on Computer Vision and Pattern Recognition*, pages 18000–18010, 2023. 5, 7, 8, 11, 12
- [6] Junyoung Chung, Caglar Gulcehre, Kyunghyun Cho, and Yoshua Bengio. Empirical evaluation of gated recurrent neural networks on sequence modeling. *arXiv preprint arXiv:1412.3555*, 2014. 6
- [7] Wenxun Dai, Ling-Hao Chen, Jingbo Wang, Jinpeng Liu, Bo Dai, and Yansong Tang. Motionlcm: Real-time controllable motion generation via latent consistency model. *arXiv preprint arXiv:2404.19759*, 2024. 8
- [8] Jacob Devlin, Ming-Wei Chang, Kenton Lee, and Kristina Toutanova. Bert: Pre-training of deep bidirectional transformers for language understanding. In *North American Chapter of the Association for Computational Linguistics*, 2019. 1
- [9] Albert Gu and Tri Dao. Mamba: Linear-time sequence modeling with selective state spaces. *arXiv preprint arXiv:2312.00752*, 2023. 8
- [10] Chuan Guo, Xinxin Zuo, Sen Wang, Shihao Zou, Qingyao Sun, Annan Deng, Minglun Gong, and Li Cheng. Action2motion: Conditioned generation of 3d human motions. In *Proceedings of the 28th ACM International Conference on Multimedia*, pages 2021–2029, 2020. 7
- [11] Chuan Guo, Shihao Zou, Xinxin Zuo, Sen Wang, Wei Ji, Xingyu Li, and Li Cheng. Generating diverse and natural 3d human motions from text. In *Proceedings of the IEEE/CVF Conference on Computer Vision and Pattern Recognition*, pages 5152–5161, 2022. 1, 2, 4, 5, 6, 7, 11
- [12] Chuan Guo, Xinxin Zuo, Sen Wang, and Li Cheng. Tm2t: Stochastic and tokenized modeling for the reciprocal generation of 3d human motions and texts. In *European Conference on Computer Vision*, pages 580–597. Springer, 2022. 1, 8
- [13] Chuan Guo, Yuxuan Mu, Muhammad Gohar Javed, Sen Wang, and Li Cheng. Momask: Generative masked modeling of 3d human motions. In *Proceedings of the IEEE/CVF Conference on Computer Vision and Pattern Recognition*, pages 1900–1910, 2024. 1, 2, 3, 4, 5, 6, 7, 8, 11, 12
- [14] Yunhui Guo, Chaofeng Wang, Stella X Yu, Frank McKenna, and Kincho H Law. Adaln: a vision transformer for multidomain learning and predisaster building information extraction from images. *Journal of Computing in Civil Engineering*, 36(5):04022024, 2022. 6
- [15] Kaiming He, Xiangyu Zhang, Shaoqing Ren, and Jian Sun. Deep residual learning for image recognition. In *Proceedings of the IEEE conference on computer vision and pattern recognition*, pages 770–778, 2016. 2, 5
- [16] Jack Hessel, Ari Holtzman, Maxwell Forbes, Ronan Le Bras, and Yejin Choi. Clipscore: A reference-free evaluation metric for image captioning. *arXiv preprint arXiv:2104.08718*, 2021. 7
- [17] Jonathan Ho and Tim Salimans. Classifier-free diffusion guidance. *arXiv preprint arXiv:2207.12598*, 2022. 12
- [18] Jonathan Ho, Ajay Jain, and Pieter Abbeel. Denoising diffusion probabilistic models. *Advances in neural information processing systems*, 33:6840–6851, 2020. 1, 2, 3, 7, 8
- [19] Biao Jiang, Xin Chen, Wen Liu, Jingyi Yu, Gang Yu, and Tao Chen. Motiongpt: Human motion as a foreign language. *Advances in Neural Information Processing Systems*, 36:20067–20079, 2023. 8
- [20] Jihoon Kim, Jiseob Kim, and Sungjoon Choi. Flame: Free-form language-based motion synthesis & editing. In *Proceedings of the AAAI Conference on Artificial Intelligence*, pages 8255–8263, 2023. 1, 8
- [21] Diederik P Kingma. Auto-encoding variational bayes. *arXiv preprint arXiv:1312.6114*, 2013. 4
- [22] Tianhong Li, Yonglong Tian, He Li, Mingyang Deng, and Kaiming He. Autoregressive image generation without vector quantization. *arXiv preprint arXiv:2406.11838*, 2024. 1, 6
- [23] Han Liang, Wenqian Zhang, Wenxuan Li, Jingyi Yu, and Lan Xu. Intergen: Diffusion-based multi-human motion generation under complex interactions. *International Journal of Computer Vision*, pages 1–21, 2024. 6
- [24] Angela S Lin, Lemeng Wu, Rodolfo Corona, Kevin Tai, Qixing Huang, and Raymond J Mooney. Generating animated videos of human activities from natural language descriptions. *Advances in neural information processing systems*, 2018. 1
- [25] Nanye Ma, Mark Goldstein, Michael S Albergo, Nicholas M Boffi, Eric Vanden-Eijnden, and Saining Xie. Sit: Exploring flow and diffusion-based generative models with scalable interpolant transformers. *arXiv preprint arXiv:2401.08740*, 2024. 5, 7, 12

- [26] Naureen Mahmood, Nima Ghorbani, Nikolaus F Troje, Gerard Pons-Moll, and Michael J Black. Amass: Archive of motion capture as surface shapes. In *Proceedings of the IEEE/CVF International Conference on Computer Vision*, pages 5442–5451, 2019. 7
- [27] Carnegie Mellon University CMU Graphics Lab motion capture library. Carnegie mellon university - cmu graphics lab - motion capture library. *Carnegie Mellon University - CMU Graphics Lab - motion capture library*, 2017. 7
- [28] William Peebles and Saining Xie. Scalable diffusion models with transformers. In *Proceedings of the IEEE/CVF International Conference on Computer Vision*, pages 4195–4205, 2023. 1, 12
- [29] Jeffrey Pennington, Richard Socher, and Christopher Manning. GloVe: Global vectors for word representation. In *Proceedings of the 2014 Conference on Empirical Methods in Natural Language Processing (EMNLP)*, pages 1532–1543, Doha, Qatar, 2014. Association for Computational Linguistics. 6
- [30] Ekkasit Pinyoanuntapong, Muhammad Usama Saleem, Pu Wang, Minwoo Lee, Srijan Das, and Chen Chen. Bamm: Bidirectional autoregressive motion model. *arXiv preprint arXiv:2403.19435*, 2024. 5, 6, 8
- [31] Ekkasit Pinyoanuntapong, Pu Wang, Minwoo Lee, and Chen Chen. Mmm: Generative masked motion model. In *Proceedings of the IEEE/CVF Conference on Computer Vision and Pattern Recognition*, pages 1546–1555, 2024. 5, 6, 7, 8, 11, 12
- [32] Matthias Plappert, Christian Mandery, and Tamim Asfour. The kit motion-language dataset. *Big data*, 4(4):236–252, 2016. 2, 7
- [33] Alec Radford, Jong Wook Kim, Chris Hallacy, Aditya Ramesh, Gabriel Goh, Sandhini Agarwal, Girish Sastry, Amanda Askell, Pamela Mishkin, Jack Clark, et al. Learning transferable visual models from natural language supervision. In *International conference on machine learning*, pages 8748–8763. PMLR, 2021. 6
- [34] Robin Rombach, Andreas Blattmann, Dominik Lorenz, Patrick Esser, and Björn Ommer. High-resolution image synthesis with latent diffusion models. In *Proceedings of the IEEE/CVF conference on computer vision and pattern recognition*, pages 10684–10695, 2022. 1, 12
- [35] David E. Rumelhart, Geoffrey E. Hinton, and Ronald J. Williams. Learning internal representations by error propagation. 1986. 1
- [36] Chitwan Saharia, William Chan, Saurabh Saxena, Lala Li, Jay Whang, Emily L Denton, Kamyar Ghasemipour, Raphael Gontijo Lopes, Burcu Karagol Ayan, Tim Salimans, et al. Photorealistic text-to-image diffusion models with deep language understanding. *Advances in neural information processing systems*, 35:36479–36494, 2022. 1
- [37] Jiaming Song, Chenlin Meng, and Stefano Ermon. Denoising diffusion implicit models. *arXiv preprint arXiv:2010.02502*, 2020. 8
- [38] Guy Tevet, Brian Gordon, Amir Hertz, Amit H Bermano, and Daniel Cohen-Or. Motionclip: Exposing human motion generation to clip space. In *European Conference on Computer Vision*, pages 358–374. Springer, 2022. 6
- [39] Guy Tevet, Sigal Raab, Brian Gordon, Yoni Shafir, Daniel Cohen-or, and Amit Haim Bermano. Human motion diffusion model. In *The Eleventh International Conference on Learning Representations*, 2023. 1, 3, 4, 7, 8, 12
- [40] Michael Tschannen, Cian Eastwood, and Fabian Mentzer. Givt: Generative infinite-vocabulary transformers. In *European Conference on Computer Vision*, pages 292–309. Springer, 2025. 6
- [41] Aaron Van Den Oord, Oriol Vinyals, et al. Neural discrete representation learning. *Advances in neural information processing systems*, 30, 2017. 2
- [42] A Vaswani. Attention is all you need. *Advances in Neural Information Processing Systems*, 2017. 1, 6
- [43] Jianrong Zhang, Yangsong Zhang, Xiaodong Cun, Shaoli Huang, Yong Zhang, Hongwei Zhao, Hongtao Lu, and Xi Shen. T2m-gpt: Generating human motion from textual descriptions with discrete representations. *arXiv preprint arXiv:2301.06052*, 2023. 1, 2, 3, 4, 5, 7, 8, 11, 12
- [44] Mingyuan Zhang, Zhongang Cai, Liang Pan, Fangzhou Hong, Xinying Guo, Lei Yang, and Ziwei Liu. Motiandiffuse: Text-driven human motion generation with diffusion model. *arXiv preprint arXiv:2208.15001*, 2022. 1, 7, 8, 12
- [45] Mingyuan Zhang, Xinying Guo, Liang Pan, Zhongang Cai, Fangzhou Hong, Huirong Li, Lei Yang, and Ziwei Liu. Remodiffuse: Retrieval-augmented motion diffusion model. In *Proceedings of the IEEE/CVF International Conference on Computer Vision*, pages 364–373, 2023. 1, 7, 8
- [46] Yaqi Zhang, Di Huang, Bin Liu, Shixiang Tang, Yan Lu, Lu Chen, Lei Bai, Qi Chu, Nenghai Yu, and Wanli Ouyang. Motiongpt: Finetuned llms are general-purpose motion generators. In *Proceedings of the AAAI Conference on Artificial Intelligence*, pages 7368–7376, 2024. 8
- [47] Zeyu Zhang, Akide Liu, Ian Reid, Richard Hartley, Bohan Zhuang, and Hao Tang. Motion mamba: Efficient and long sequence motion generation. In *European Conference on Computer Vision*, pages 265–282. Springer, 2025. 1, 8
- [48] Chongyang Zhong, Lei Hu, Zihao Zhang, and Shihong Xia. Att2m: Text-driven human motion generation with multi-perspective attention mechanism. In *Proceedings of the IEEE/CVF International Conference on Computer Vision*, pages 509–519, 2023. 8

# Rethinking Diffusion for Text-Driven Human Motion Generation

## Supplementary Material

We further discuss our proposed approach with the following supplementary materials:

- Appendix A: Detailed Deduction
- Appendix B: Implementation Details
- Appendix C: Additional Quantitative Results
- Appendix D: Temporal Editing
- Appendix E: Additional Qualitative Results
- Appendix F: Limitations

### A. Detailed Deduction

#### A.1. Detailed Deduction for Eq. (4)

In paper, we define  $\delta_{\mathbf{x}_0}$  and  $\delta_\epsilon$  to be:

$$\delta_\epsilon = \|\epsilon_\theta(\mathbf{x}_t, t) - \epsilon\|_2^2 \quad (20)$$

and

$$\delta_{\mathbf{x}_0} = \|\mathbf{x}'_0 - \mathbf{x}_0\|_2^2 \quad (21)$$

Since in diffusion-based methods, in each step, diffusion-based methods reconstruct the original motion by:

$$\mathbf{x}'_0 = \frac{1}{\sqrt{\bar{\alpha}_t}}(\mathbf{x}_t - \sqrt{1 - \bar{\alpha}_t}\epsilon_\theta(\mathbf{x}_t, t)) \quad (22)$$

where  $\epsilon_\theta(\mathbf{x}_t, t)$  is the model’s prediction of the noise  $\epsilon$ . Then we have:

$$\delta_{\mathbf{x}_0} = \left\| \frac{1}{\sqrt{\bar{\alpha}_t}}(\mathbf{x}_t - \sqrt{1 - \bar{\alpha}_t}\epsilon_\theta(\mathbf{x}_t, t)) - \mathbf{x}_0 \right\|_2^2$$

If we substitute  $\mathbf{x}_0$  from Eq. (1):

$$\begin{aligned} \delta_{\mathbf{x}_0} &= \left\| \frac{1}{\sqrt{\bar{\alpha}_t}}(\sqrt{\bar{\alpha}_t}\mathbf{x}_0 + \sqrt{1 - \bar{\alpha}_t}\epsilon) \right. \\ &\quad \left. - \frac{1}{\sqrt{\bar{\alpha}_t}}(\sqrt{1 - \bar{\alpha}_t}\epsilon_\theta(\mathbf{x}_t, t)) - \mathbf{x}_0 \right\|_2^2 \\ &= \left\| \mathbf{x}_0 + \frac{\sqrt{1 - \bar{\alpha}_t}}{\sqrt{\bar{\alpha}_t}}(\epsilon - \epsilon_\theta(\mathbf{x}_t, t)) - \mathbf{x}_0 \right\|_2^2 \\ &= \left\| \frac{\sqrt{1 - \bar{\alpha}_t}}{\sqrt{\bar{\alpha}_t}}(\epsilon - \epsilon_\theta(\mathbf{x}_t, t)) \right\|_2^2 \\ &= \left\| \frac{\sqrt{1 - \bar{\alpha}_t}}{\sqrt{\bar{\alpha}_t}} \right\|_2^2 \delta_\epsilon \end{aligned} \quad (23)$$

an standard error relation  $\delta_\epsilon \rightarrow \delta_{\mathbf{x}_0}$  if  $\mathbf{x}_0$  is processed correctly which should only responds to time coefficient  $\bar{\alpha}$ .

Table A1. **Reconstruction Results** of latent encoders in our method vs baseline methods on HumanML3D [11] data. The AutoEncoder in our method exhibits better reconstruction results.

Methods	FID ↓	MPJPE ↓	R-Precision ↑		
			Top 1	Top 2	Top 3
VQ-VAE [43]	0.081±.001	72.6±.001	0.483±.003	0.680±.003	0.780±.002
RVQ-VAE [13]	0.029±.001	31.5±.001	0.497±.002	0.693±.003	0.791±.002
VAE [5]	0.023±.001	13.7±.001	0.499±.002	0.695±.003	0.791±.003
AE (Ours)	<b>0.004±.001</b>	<b>1.0±.001</b>	<b>0.502±.003</b>	<b>0.696±.002</b>	<b>0.793±.002</b>

Table A2. **Model Scaling** results of our model. Increasing model size results in better overall performance on HumanML3D.

Size	Transformer	MLP	FID ↓	R-Precision ↑		
				Top 1	Top 2	Top 3
S	6 head 384 dim	3 layers 1024 dim	0.278	0.481	0.676	0.779
	12 head 768 dim	8 layers 1280 dim	0.189	0.479	0.676	0.779
M	6 head 384 dim	8 layers 1280 dim	0.189	0.479	0.676	0.779
	12 head 768 dim	8 layers 1280 dim	0.173	0.477	0.679	0.780
L	6 head 384 dim	12 layers 1536 dim	0.137	0.485	0.683	0.785
	12 head 768 dim	12 layers 1536 dim	0.125	0.487	0.685	0.785
XL	16 head 1024 dim	16 layers 1792 dim	0.116	0.492	0.690	0.790

### B. Implementation Details

For our method, the AutoEncoder is a 3-layer ResNet-based encoder-decoder with a hidden dimension of 512 and a total downsampling rate of 4. For the generation branch, we utilize a single-layer AdaLN-Zero transformer encoder with a hidden dimension of 1024 and 16 heads as our masked autoregressive transformer. The diffusion MLPs consist of 16 layers with a hidden dimension of 1792. We also present the model scalability results in Appendix C.2.

During training, we use the AdamW optimizer with  $\beta_1 = 0.9$  and  $\beta_2 = 0.99$ . Following prior works [11, 13, 31, 43], the batch size is set to 256 and 512 for training the AutoEncoder on the HumanML3D and KIT-ML datasets, respectively, with each sample containing 64 frames. For training the generation branch, the batch size is set to 64 for HumanML3D and 16 for KIT-ML, with a maximum sequence length of 196 frames. The learning rate is set at  $2 \times 10^{-4}$  with a linear warmup of 2000 steps. We train the AutoEncoder for 50 epochs and modify the learn-

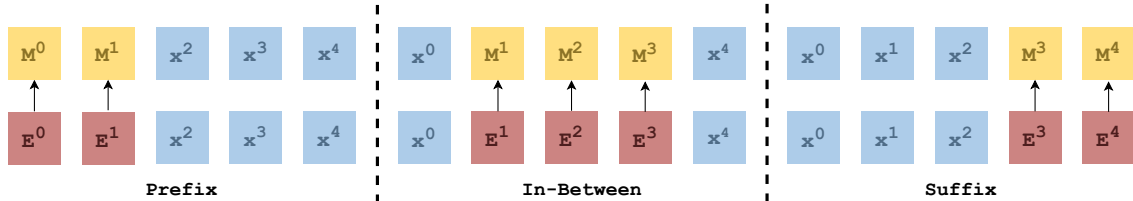


Figure A1. **Our Method’s Temporal Editing** process, including prefix, in-between, and suffix editing. The editing latents (red color) are treated as masked latents (yellow color). The sequence is then input into the generation branch in Fig. 3 to generate edited latents conditioned on the editing textual instruction and non-edit latents (blue color).

Table A3. **Average Inference Time Results Comparison** between our method and baseline methods.

Methods	MDM [39]	MotionDiffuse [44]	T2M-GPT [43]	MLD [5]	MMM [31]	MoMask [13]	Ours
AIT	14.31s	7.35s	0.32s	0.21s	0.06s	0.04s	2.4s

ing rate to decay by a factor of 20 or 10 at milestones of 150,000 and 250,000 iterations for HumanML3D and KIT-ML datasets, respectively. For the generation branch, the learning rate decays by a factor of 0.1 at 50,000 iterations for HumanML3D and 20,000 iterations for KIT-ML during a 500-epoch training process. Following image diffusion works [25, 28, 34], we also incorporate exponential moving average (EMA) when updating the model parameters to achieve more stable performance. In the generation process, for HumanML3D, the CFG [17] scale is set to 4.5 and for KIT, the conditioning scale is set to 2.5.

## C. Additional Quantitative Results

### C.1. AutoEncoder Reconstruction Results

In Tab. A1, we present the reconstruction results of VQ-VAE from T2M-GPT [43], RVQ-VAE from MoMask [13], VAE from MLD [5], and the AutoEncoder (AE) in our method. Our AutoEncoder has much better reconstruction capability than baseline methods, which ultimately benefits both diffusion model training and sampling.

### C.2. Model Scalability

We train six versions of our proposed model (DDPM approach), varying three transformer sizes and four diffusion MLP sizes (S, M, L, XL). These models range in size from around 30M, 100M, 180M, to 290M parameters. The performance results are summarized in Tab. A2. We observe that increasing the model size, particularly the diffusion MLPs size, improves overall generation performance, especially in terms of FID.

## D. Temporal Editing

Our method is capable of performing temporal editing in a zero-shot manner (*i.e.* utilizing the model trained for text-to-motion generation without any editing-specific fine-tuning). In our method, temporal motion editing is easily achieved by treating the latents that need to be edited as masked latents and then generating motions following our

standard generation procedure in Sec. 3.2 which is conditions on the unmasked tokens (*i.e.* non-edit latents) and the editing textual instructions. We visually illustrate this process in Fig. A1 and we also include temporal editing results in the locally-run, anonymous HTML file referenced in Appendix E.

## E. Additional Qualitative Results

Beyond the qualitative results presented in the main paper, we also provide comprehensive video visualizations hosted on a locally-run, anonymous HTML webpage to further demonstrate the effectiveness of our approach. These visualizations include additional comparisons with state-of-the-art baseline methods, showcasing that our method generates more realistic motions and adheres more closely to textual instructions. We also present motion videos from our ablation studies to highlight the significance of each component. For example, omitting motion representation reformulation results in noticeable shaking and poses inaccuracies, while excluding the autoregressive modeling approach leads to worse textual instructions following. Furthermore, we also demonstrate our method’s capability for temporal editing with prefix, in-between, and suffix editing results. Finally, we provide additional visualizations to illustrate that our method can generate a wide range of diverse and contextually appropriate motions.

## F. Limitations

Since our method incorporates both standard reverse-diffusion processes (over  $T$  time steps) and autoregressive generation within each step to produce high-quality and diverse motion, it inherently requires more time for motion generation compared to some baseline methods (*e.g.*, MoMask, MMM). To provide a clear comparison, in Tab. A3, we report the efficiency of motion generation in terms of average inference time (AIT) over 100 samples on a single Nvidia 4090 device. Notably, our method still outperforms several diffusion-based methods, *e.g.* MDM and MotionDiffuse, in generation speed by a significant margin. For

future work, we aim to explore strategies to optimize and accelerate both standard reverse-diffusion and autoregressive generation processes.